Nonmydriatic fluorescence-based quantitative imaging of human macular pigment distributions

Mohsen Sharifzadeh

Department of Physics, University of Utah, Salt Lake City, Utah 84112

Paul S. Bernstein

Department of Ophthalmology and Visual Sciences, Moran Eye Center, University of Utah School of Medicine, Salt Lake City, Utah 84132

Werner Gellermann

Department of Physics, University of Utah, Salt Lake City, Utah 84112

Received October 25, 2005; revised April 19, 2006; accepted April 25, 2006; posted May 17, 2006 (Doc. ID 65542)

We have developed a CCD-camera-based nonmydriatic instrument that detects fluorescence from retinal lipofuscin chromophores ("autofluorescence") as a means to indirectly quantify and spatially image the distribution of macular pigment (MP). The lipofuscin fluorescence intensity is reduced at all retinal locations containing MP, since MP has a competing absorption in the blue–green wavelength region. Projecting a large diameter, 488 nm excitation spot onto the retina, centered on the fovea, but extending into the macular periphery, and comparing lipofuscin fluorescence intensities outside and inside the foveal area, it is possible to spatially map out the distribution of MP. Spectrally selective detection of the lipofuscin fluorescence reveals an important wavelength dependence of the obtainable image contrast and deduced MP optical density levels, showing that it is important to block out interfering fluorescence contributions in the detection setup originating from ocular media such as the lens. Measuring 70 healthy human volunteer subjects with no ocular pathologies, we find widely varying spatial extent of MP, distinctly differing distribution patterns of MP, and strongly differing absolute MP levels among individuals. Our population study suggests that MP imaging based on lipofuscin fluorescence is useful as a relatively simple, objective, and quantitative noninvasive optical technique suitable to rapidly screen MP levels and distributions in healthy humans with undilated pupils.

OCIS codes: 170.0170, 170.1610, 170.3890, 170.4580, 300.6450, 330.4300.

1. INTRODUCTION

Currently there is strong interest in developing noninvasive detection techniques for macular pigment (MP) in the living human retina. Composed of the carotenoid compounds lutein and zeaxanthin, MP is thought to play a protective role in the prevention or delay of age-related macular degeneration (AMD), the leading cause of irreversible blindness in the elderly in the Western world.[1,2] Epidemiological studies analyzing carotenoid levels via dietary surveys and serum assays have shown that there is an inverse correlation between high dietary intakes and blood levels of lutein and zeaxanthin and risk of advanced AMD.[3–6] Furthermore, recent high performance liquid chromatography (HPLC) analysis of human cadaver eyes with and without a known history of AMD has demonstrated a correlation between levels of lutein and zeaxanthin and AMD,[7] and recent flicker photometry and resonance Raman clinical studies reached the same conclusion, although a reflectometry study did not.[8–10] The development of noninvasive methods capable of assessing MP levels in living humans, in particular objective methods that can quantify and spatially resolve MP distributions reliably and rapidly in large populations, would be of tremendous benefit to epidemiological research on AMD. They could be used, for example, in large-scale monitoring studies of dietary and/or nutritional interventions designed to raise MP levels, and they could potentially help protect a large fraction of the population from developing this debilitating disease.

MP is concentrated in the ~1-mm-diameter region of the retina that provides high-acuity vision. It usually peaks in the center of the macula, the foveola, and drops off rapidly with increasing eccentricity. Absolute concentrations of MP at this site are very high compared with those at other tissue sites, corresponding typically to 10–30 ng per macular punch biopsy (~5 mm diameter). The spectral absorption behavior is shown in Fig. 1 for an excised macula that was measured through a 1 mm aperture; it shows that MP optical density levels in the peak of the absorption near 460 nm are typically very strong. In spite of the very thin retinal tissue layer, the optical density reaches an average value of ~0.3 above background, which explains the origin of the strong yellow coloration of the macula. Comparing the optical absorption of the macula with lutein and zeaxanthin solutions, one finds that the absorption behavior is remarkably similar, including the appearance of vibronic substructure, and that there is little overlap with potentially confounding other chromophores in the intact retina.[11]

Optical excitation of MP leads to only very weak fluo-

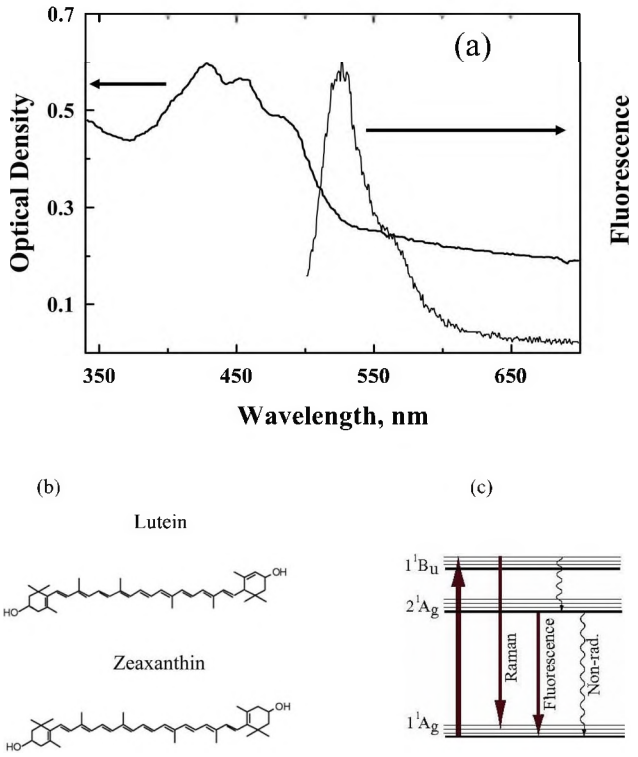

Fig. 1. (a) Absorption spectrum of an excised, flat-mounted, human retina in the blue–green wavelength region, showing typical absorption characteristics of carotenoid macular pigment (MP) (solid curve at left). The retinal pigment epithelium (RPE) of the retina was removed for this measurement, and the spectrum was measured through a 1 mm aperture. The tissue absorption is remarkably similar in spectral shape to the absorption of a lutein/zeaxanthin solution, including the appearance of vibronic absorption substructure. The solid curve at right shows the fluorescence spectrum of a solution of lutein, obtained under excitation at 488 nm. (b) Molecular structure of lutein and zeaxanthin. (c) Energy level diagram of long-chain conjugated carotenoids such as lutein or zeaxanthin, with optical and nonradiative transitions indicated as arrows.

rescence, since the excited lutein and zeaxanthin molecules relax very rapidly (within 200–250 fs) to a lower lying excited state from which emission of light is parity forbidden [see Fig. 1(c)]. The unusual ordering of the energy states is a unique feature of the polyenelike, π-conjugated carotenoids having a large number of conjugated C=C double bonds [10 and 11 in lutein and zeaxanthin, respectively; see Fig. 1(b)]. In fact, the quantum efficiency for a radiative transition from the $2\ ^1A_g$ excited state to the $1\ ^1A_g$ ground state is estimated to be as low as 10^{-5} to 10^{-4}.[12] Therefore relaxation of the excited molecule back to the ground state occurs mostly via nonradiative transitions. The weak emission, observable only with very sensitive detection, has a small Stokes shift, and it occurs in the green wavelength range centered at ~530 nm, as shown in Fig. 1.

Due to the weak fluorescence transitions, direct detection of MP using lutein or zeaxanthin fluorescence has not been realized to date. However, the virtual absence of intrinsic MP fluorescence makes it possible to detect instead the resonance Raman transitions of MP, even in living human eyes,[11,13] which would otherwise be masked beyond detection by the fluorescence background. Raman detection methods have the benefit of extremely high specificity for lutein and zeaxanthin, and therefore for MP (see below). However, detecting only the absolute amount of MP, the Raman response is attenuated to some degree by the combined absorption and scattering of anterior ocular media, predominantly the lens.[11,14,15]

One of the MP imaging approaches is based on fundus reflectance techniques. There are two variants in which this method is implemented. In one variant, the reflectance of a broadband light source from the sclera is compared for foveal and perifoveal spots, and the spectral contribution of the absorbance by MP is calculated. In a second variant, no reference at a peripheral site is needed. Only a foveal field is used, and MP levels are derived from a model fit that takes into account the absorption and scattering coefficients of all retinal layers traversed in a double-path succession by the light.[16–18] A review of the technology can be found in Ref. 19. A recently developed state of the art reflection device based on an imaging spectrograph, white light excitation source, and CCD camera detection, which performs single reflection measurements within a fraction of a second, with additional cone-photoreceptor directionality, has been described by Zagers *et al.*[20] Some reflectance-based imaging variants are based on scanning laser ophthalmoscopes (SLOs).[21] Argon laser lines at 488 and 514 nm are used to generate monochromatic digital reflection images from the retina at MP "on peak" and "off peak" spectral absorption positions, which are then digitally subtracted to display the MP absorption distribution. Berendschot and colleagues have compared direct reflectance and digital subtraction SLO methods in a lutein supplementation study[22] and found that an SLO provided the most reliable data. They also found that MP optical density (O.D.) rises by approximately 5% per month in response to daily lutein supplementation. Using a modified confocal SLO, Wüstemeyer *et al.* found reduced MP levels in AMD subjects as compared with healthy subjects,[23] and Schweitzer *et al.* found that the effects of lutein supplementation on MP levels could be tracked with SLO images generated by single-wavelength, 488 nm excitation.[24] Population studies employing reflectance techniques have reported significantly varying results regarding MP levels, depending on the size of the tested foveal fields, instrumental aspects, and tissue models used for data reduction. In a population study of 159 subjects, measuring a foveal area of 2°, an average MP O.D. value of 0.23 was found.[25] In another random population-based sample of 435 subjects, with subjects older then 55 yr, measured over a 2.3° test field, an average MP O.D. level of 0.33 was determined.[10] In another large sample, involving 138 subjects and a 1.9° test field, an average MP O.D. level of 0.48 was found.[19] In all these studies no age effect was observed. While reflectance-based MP imaging is evolving as a viable clinical technique for subjects of all ages, a drawback of the technology is seen in the need for eyes in mydriasis.[19] The reasons for the large variations in average MP levels remain unclear.

A further quantitative imaging technique for MP distributions is based on resonance Raman spectroscopy.[11,26] This method detects the light that is Raman scattered from the MP carotenoid molecules at their 1525 cm^{-1}

C=C double bond stretch frequency under resonant excitation in the MP absorption band. The Raman method measures the response of MP directly, has a very high molecule specificity, and has been validated by correlating Raman-image-derived MP distributions with HPLC-derived MP levels in excised human eye cups and living monkey eyes.[11] Very recently it has been possible to extend Raman imaging to living human eyes. Highly MP-specific digital Raman intensity maps can be obtained with high spatial resolution through undilated eyes within a fraction of a second.[27] The validity of *in vivo* methods used to measure MP is currently being debated in the literature.[14,15]

2. MACULAR PIGMENT DETECTION BASED ON LIPOFUSCIN SPECTROSCOPY

In this work, we investigate the potential merits and drawbacks of lipofuscin fluorescence spectroscopy ("autofluorescence spectroscopy"), which appears to be yet another promising approach for the quantitative detection and imaging of MP. The method was first proposed some time ago by Delori, who used it to determine the integrated single-path absorption of MP.[28] A comparison of the technique with nonimaging heterochromatic flicker photometry and reflectometry in a relatively large population sample revealed reasonable correlations of MP levels, although there were significant and systematic differences.[25] Interestingly, the average MP optical density based on lipofuscin spectroscopy was 0.48 for a 2° test field, whereas reflectance techniques yielded only about half that value, 0.23, and the psychophysical technique gave a value in between, i.e., 0.37. Recently, the method has been expanded to an imaging configuration using a customized confocal SLO,[29,30] with measured test fields as large as 40°, and to an imaging configuration that uses a modified fundus camera coupled to a CCD camera.[31] All reported imaging studies had to be carried out with dilated pupils. Robson and co-workers, using 488 nm laser excitation and a short-wavelength cutoff filter of 521 nm in their lipofuscin-based measurements, compared the obtained MP densities with MP levels measured with motion photometry for eight subjects.[29] They observed good correlation but found the lipofuscin-based MP levels to be a systematic factor of 1.7 lower than the psychophysically derived levels. Most importantly, their study demonstrated large intersubject differences in macular pigmentation in terms of peak density, extent of lateral distribution, and total amount. Furthermore, the authors demonstrated that large spatial MP distributions can lead to an underestimate of MP levels in psychophysical methods if the peripheral reference point is chosen too close to the fovea. Trieschmann and co-workers used a confocal SLO in combination with 488 nm laser excitation and 500 nm barrier filter detection, and they measured MP distributions in a large population sample including 400 subjects with the age range 41–90 yr.[30] They showed that subjects fall into one of four classes of MP distributions that are usable as a grading system. Due to differences in central and paracentral MP levels, total MP concentration decreases from type 1 to the other types. Importantly, these authors observed reduced levels of MP in a subgroup of subjects having early AMD, showing effects such as drusen, retinal pigment epithelium (RPE) proliferation, and atrophy, and speculated that subjects with type 3 and 4 MP distributions may have increased risk for AMD development. However, questions remain about the measurement approach, since these authors did not justify the omission of a measurement at a second reference wavelength that is not absorbed by the MP. Delori involved 38 subjects in his imaging study,[31] employing in his instrumentation dual-wavelength, broadband excitation centered at 470 and 550 nm, respectively (FWHM ~30 nm), and a barrier filter limiting lipofuscin emission to wavelengths above 590 nm. He found that lipofuscin-based methods using only one excitation wavelength (460 nm) would overestimate the MP levels by 0.22. Regarding age effects, he observed a slight increase of MP levels with age. Recently, further SLO-based autofluorescence studies have been carried out by Wüstemeyer *et al.*,[32] Hammer *et al.*,[33] and Schweitzer *et al.*[34]

Human RPE contains the age pigment lipofuscin, which accumulates in the lysosomal body of the RPE cells.[35] Two components of lipofuscin exist that absorb strongly in the blue wavelength region and emit strongly in the orange–red region. They are two isomers of a bis-substituted pyridinium ring, termed A2E and iso-A2E, respectively.[36] The structure of the molecules, their optical transitions,[37] and their associated energy level scheme are shown in Fig. 2. The absorption spectrum of A2E partially overlaps with the absorption spectrum of the macular carotenoids, and its emission spectrum is broad, extending to wavelengths well beyond the absorption of carotenoids, as shown in Fig. 2. It is possible, therefore, to excite the A2E emission within and outside the absorption range of MP. Similar to lutein and zeaxanthin, A2E has a conjugated carbon backbone. However, the conjugation length is shorter, interrupted by the central pyridinium ring, which shortens the conjugated carbon bond chain to two smaller chains with five double bonds each. This leads to an emission with a quantum efficiency of 10^{-2},[37] which is about 3 orders of magnitude stronger than that reported for lutein and zeaxanthin.[12] The *in vivo* excitation spectrum of fundus autofluorescence is much broader than that of A2E, suggesting that other lipofuscin fluorophores contribute to fundus autofluorescence.[38] Regarding its spatial distribution, the data of Ref. 38 show that the lipofuscin fluorescence at 15° from the fovea is 1.4–1.7 times higher than at the fovea and that there is a gradual increase in lipofuscin fluorescence with increasing eccentricity.

For indirect MP detection, the fluorescence of lipofuscin is excited at two wavelengths: one wavelength that overlaps both the MP and lipofuscin absorption and another, longer wavelength that lies outside the MP absorption range but that still excites the lipofuscin emission on the shoulder of the lipofuscin absorption. The MP absorption can then be approximated from the difference in lipofuscin fluorescence intensities at foveal and perifoveal locations.[25,28] Imaging approaches have used laser excitations that raster scan across the macula and beyond[29,30] or broadband excitation with beam diameters that are centered on the fovea and extend into the periphery.[31] MP optical density maps are usually generated by referencing

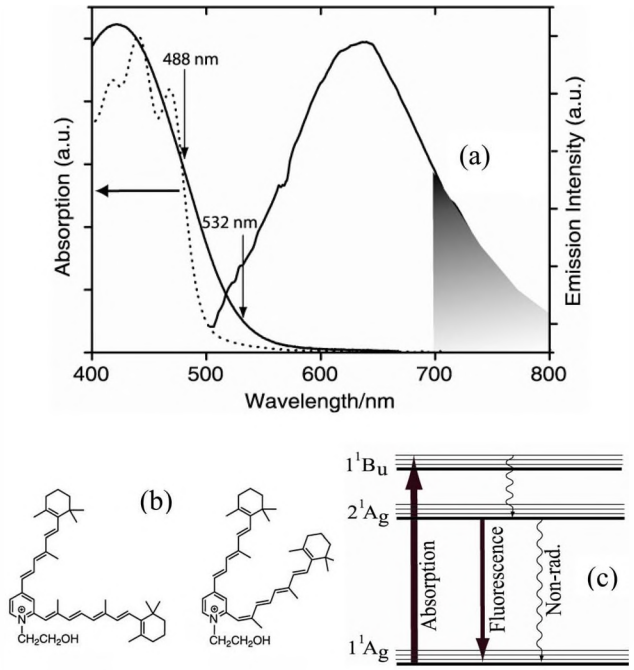

Fig. 2. (a) Absorption and emission spectra of a methanolic solution of A2E, the main fluorophore of lipofuscin, shown as solid curves at the left and right sides of the panel, respectively. The absorption transition between the lowest energy levels occurs in a broadband centered at 440 nm. Optical excitation leads to a strong emission centered at 660 nm. The overlapping absorption of MP is indicated as a dotted curve. The gray shaded area ($\lambda > 700$ nm) indicates the lipofuscin fluorescence range used for indirect detection and imaging of MP distributions. (b) Molecular structures of (left) A2E and (right) iso-A2E. (c) Energy level diagram with optical transitions shown as arrows. Compared with carotenoids, the fluorescence transition is stronger in the A2E molecules due to their shorter conjugation length, which is interrupted by the central pyridinium ring.

the MP levels in the macular region to a perifoveal reference point at about 7° eccentricity. Compared with MP Raman detection, which uses backscattering of excitation light from the MP-containing Henle fiber layer, and therefore is not influenced by deeper retinal layers, lipofuscin-based MP detection has to use a light source in the deep RPE layer for that purpose, and it has to take into account additional absorption and emission effects of these layers and their fluorophores, as shown in Fig. 3(a).

As seen in resonance Raman detection experiments of MP, which detect the spectrally sharp C=C double bond 1525 cm^{-1} stretching vibration Raman responses of lutein and zeaxanthin (which occur at 527 nm under 488 nm excitation), a strong fluorescence background is superimposed on the Raman response in the 530 nm region.[11] This fluorescence background varies strongly from subject to subject and exceeds in strength the background level expected from intrinsic lutein or zeaxanthin (MP) fluorescence. This background is a combination of lipofuscin fluorescence and fluorescence from anterior ocular media. In Raman detection, the broad fluorescence background can be easily fitted with a higher order polynomial and subtracted from the measured spectra. In lipofuscin-based MP measurements, however, these extra fluorescence responses can be expected to play an interfering role. It is therefore essential to establish the merits and limitations of the lipofuscin method.

The optical layers of interest traversed by the excitation light and the lipofuscin fluorescence are sketched in Fig. 3(b). The fluorescence intensity in 180° detection geometry, I_{Det}, measured at a selected wavelength λ in the visible/near IR wavelength range, is in general given by

$$I_{Det}(\lambda) = I_L(\lambda)T_{PR}(\lambda)T_{MP}(\lambda)T_{OM}(\lambda) + I_{OM}(\lambda), \qquad (1)$$

where $T(\lambda)$ is the transmission of the respective layer corresponding to photoreceptors (PR), macular pigment (MP), and anterior ocular media (OM) at the fluorescence wavelength λ. I_L is the lipofuscin fluorescence originating in the fovea, and $I_{OM}(\lambda)$ is the potentially overlapping fluorescence intensity of the ocular media layer at λ.

It is safe to assume that the photoreceptors do not generate any fluorescence, but their absorption cannot be neglected, in general. Under excitation with I_{exc} at wavelength λ_{exc}, the lipofuscin fluorescence intensity $I_L(\lambda)$ is correlated with I_{exc} according to

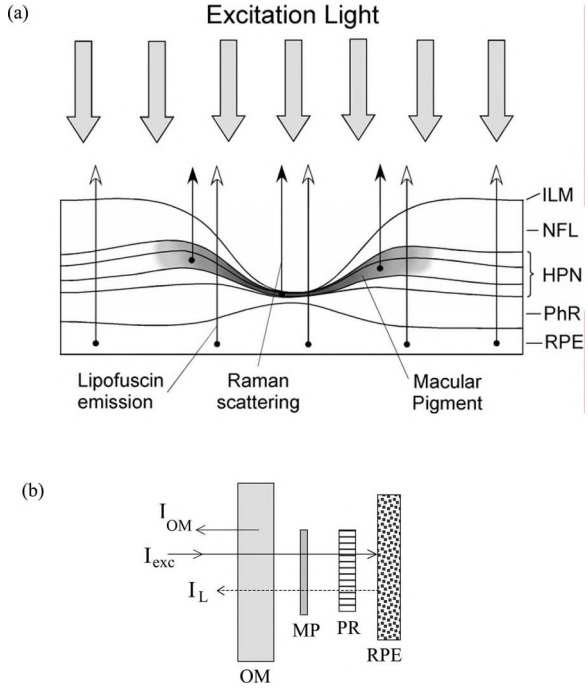

Fig. 3. (a) Schematic representation of retinal layers participating in light absorption, transmission, and scattering of excitation and emission light in the macular region. ILM, inner limiting membrane; NFL, nerve fiber layer; HPN, Henle fiber, plexiform, and nuclear layers; PhR, photoreceptor layer; RPE, retinal pigment epithelium. In Raman scattering, the scattering response originates from the MP, which is located anteriorly to the photoreceptor layer. The influence of deeper fundus layers such as the RPE is avoided. In lipofuscin spectroscopy, light emission is generated from lipofuscin in the RPE layer to generate an intrinsic "light source" for single-path absorption measurements of anteriorly located MP layers. Using an excitation beam diameter exceeding the spatial extent of MP, the MP distribution can be quantified and spatially imaged (see the text). (b) Schematics of anterior optical media and retinal layers traversed by excitation laser light, fluorescence from anterior optical media, and fluorescence from lipofuscin. I_{exc} excitation light; I_L, lipofuscin fluorescence; OM, ocular media; MP, macular pigment; PR, photoreceptors; RPE, retinal pigment epithelium; I_{OM}, fluorescence from ocular media.

$$I_L(\lambda_{exc},\lambda) = \eta_L(\lambda_{exc},\lambda) I_{exc}(\lambda_{exc}) T_{OM}(\lambda_{exc}) T_{MP}(\lambda_{exc}) T_{PR}(\lambda), \tag{2}$$

and I_{OM} is correlated with I_{exc} according to

$$I_{OM}(\lambda_{exc},\lambda) = \eta_{OM}(\lambda_{exc},\lambda) I_{exc}(\lambda_{exc})(1 - T_{OM}), \tag{3}$$

where $\eta_L(\lambda,\lambda_{exc})$ and $\eta_{OM}(\lambda,\lambda_{exc})$ are the fluorescence quantum efficiencies, respectively, of lipofuscin and the anterior ocular media.

Inserting Eqs. (2) and (3) into Eq. (1), one obtains

$$\begin{aligned} I_{Det}(\lambda_{exc},\lambda) = {} & \eta_{MP}(\lambda_{exc},\lambda) I_{exc}(\lambda_{exc}) T_{OM}(\lambda_{exc}) T_{MP}(\lambda_{exc}) \\ & \times T_{PR}(\lambda_{exc}) T_{OM}(\lambda) T_{MP}(\lambda) T_{PR}(\lambda) \\ & + \eta_{OM}(\lambda_{exc},\lambda) I_{exc}(\lambda_{exc})[1 - T_{OM}(\lambda)]. \end{aligned} \tag{4}$$

In general, it is impossible to extract the isolated MP transmission (absorption) from this complex relation between detector intensity and transmission/fluorescence terms of all layers. However, adopting a string of assumptions and approximations,[25] it becomes possible to eliminate, in first order, several unwanted terms in Eq. (4) and to derive an approximation for the MP transmission (absorption) difference between fovea and perifovea.

First, as substantiated below (Section 3), it is possible to largely block the detection of optical media fluorescence by limiting the detection of lipofuscin fluorescence to near IR wavelengths. Only under this condition can the second term in Eq. (4) be ignored. Second, it is useful to reference the detected luminescence in the fovea to a measurement in the perifovea and to determine this ratio for two excitation wavelengths λ_1 and λ_2 near the peak and just outside the MP absorption band, respectively. For the ratios of the MP transmissions in perifovea and fovea at the two wavelengths one then obtains

$$\begin{aligned} & \left[\frac{I^P_{Det}(\lambda_1,\lambda)}{I^F_{Det}(\lambda_1,\lambda)}\right] \Bigg/ \left[\frac{I^P_{Det}(\lambda_2,\lambda)}{I^F_{Det}(\lambda_2,\lambda)}\right] \\ & = \left[\frac{\eta^P_{MP}(\lambda_1,\lambda)}{\eta^F_{MP}(\lambda_1,\lambda)} \Bigg/ \frac{\eta^P_{MP}(\lambda_2,\lambda)}{\eta^F_{MP}(\lambda_2,\lambda)}\right] \left[\frac{I^P_{exc}(\lambda_1)}{I^F_{exc}(\lambda_1)} \Bigg/ \frac{I^P_{exc}(\lambda_2)}{I^F_{exc}(\lambda_2)}\right] \\ & \times \left[\frac{T^P_{MP}(\lambda_1)}{T^F_{MP}(\lambda_1)} \frac{T^P_{OM}(\lambda_1)}{T^F_{OM}(\lambda_1)} \frac{T^P_{PR}(\lambda_1)}{T^F_{PR}(\lambda_1)}\right] \Bigg/ \\ & \left[\frac{T^F_{MP}(\lambda_2)}{T^F_{MP}(\lambda_2)} \frac{T^P_{OM}(\lambda_2)}{T^F_{OM}(\lambda_2)} \frac{T^P_{PR}(\lambda_2)}{T^F_{PR}(\lambda_2)}\right]. \end{aligned} \tag{5}$$

If one assumes that the lipofuscin composition is constant across the posterior pole, the quantum efficiency ratio term $[\eta^P_{MP}(\lambda_1,\lambda)/\eta^F_{MP}(\lambda_1,\lambda)]/[\eta^P_{MP}(\lambda_2,\lambda)/\eta^F_{MP}(\lambda_2,\lambda)]$ is eliminated. If one further assumes that there is no difference between foveal and perifoveal lens transmissions, the lens transmission terms cancel out. Furthermore, if one ensures that the excitation light beam profiles are identical for the two wavelengths, they cancel out, too. One then obtains the much simplified expression

$$\begin{aligned} & \left[\frac{I^P_{Det}(\lambda_1,\lambda)}{I^F_{Det}(\lambda_1,\lambda)}\right] \Bigg/ \left[\frac{I^P_{Det}(\lambda_2,\lambda)}{I^F_{Det}(\lambda_2,\lambda)}\right] \\ & = \left[\frac{T^P_{MP}(\lambda_1)}{T^F_{MP}(\lambda_1)} \Bigg/ \frac{T^P_{MP}(\lambda_2)}{T^F_{MP}(\lambda_2)}\right] \left[\frac{T^P_{PR}(\lambda_1)}{T^F_{PR}(\lambda_1)} \Bigg/ \frac{T^P_{PR}(\lambda_2)}{T^F_{PR}(\lambda_2)}\right]. \end{aligned} \tag{6}$$

Referencing the transmissions of the excitation light at the λ_1 and λ_2 positions to the transmission values in the peak of the MP absorption band, 460 nm, with respective extinction coefficients $K_{MP}(\lambda_1)$ and $K_{MP}(\lambda_2)$, where

$$T^{P,F}_{MP}(\lambda_1) = T^{P,F}_{MP}(460)^{K(\lambda_1)}, \qquad T^{P,F}_{MP}(\lambda_2) = T^{P,F}_{MP}(460)^{K(\lambda_2)},$$

the right side of Eq. (6) reduces to $[T^P_{MP}(460)/T^F_{MP}(460)]^{[K_{MP}(\lambda_1)-K_{MP}(\lambda_2)]}$. With O.D.$=\log(1/T)$, and solving for the MP optical density difference, this can be written as

$$\begin{aligned} & \text{O.D.}^F_{MP}(\lambda_{460}) - \text{O.D.}^P_{MP}(\lambda_{460}) \\ & = \frac{1}{\Delta K}\left\{\log\left[\frac{I^P_{Det}(\lambda_1,\lambda)}{I^F_{Det}(\lambda_1,\lambda)}\right] - \log\left[\frac{I^P_{Det}(\lambda_2,\lambda)}{I^F_{Det}(\lambda_2,\lambda)}\right]\right\} \\ & - \frac{1}{\Delta K}\log\left[\frac{T^P_{PR}(\lambda_1)}{T^F_{PR}(\lambda_1)} \Bigg/ \frac{T^P_{PR}(\lambda_2)}{T^F_{PR}(\lambda_2)}\right]. \end{aligned} \tag{7}$$

If one assumes in addition that the photoreceptors can be completely bleached in the measurements ($T_{PR}=100\%$), the second term can be neglected. Then the MP optical density difference between fovea and perifovea is given by

$$\begin{aligned} \text{O.D.}^F_{MP}(\lambda_{460}) - \text{O.D.}^P_{MP}(\lambda_{460}) = \frac{1}{\Delta K}\Bigg\{ & \log\left[\frac{I^P_{Det}(\lambda_1,\lambda)}{I^F_{Det}(\lambda_1,\lambda)}\right] \\ & - \log\left[\frac{I^P_{Det}(\lambda_2,\lambda)}{I^F_{Det}(\lambda_2,\lambda)}\right]\Bigg\}, \end{aligned} \tag{8}$$

i.e., it can be approximated by the log differences of foveal and perifoveal fluorescence intensities.

It should be mentioned that besides lipofuscin detection at near IR wavelength, other approaches are possible to minimize the effects of media fluorescence. These include confocal optics, separation of excitation and detection beams through the lens, and correction for lens fluorescence.

It is instructive to compare the derived expressions with the expression for the MP signal intensity obtained with the Raman method.[11] Since the Raman response originates directly in the MP layer, deeper layers do not play a role in the excitation and emission paths. Only the anterior optical media are traversed, resulting in

$$\begin{aligned} I_S = {} & T_{OM}(\lambda_{exc}) T_{OM}(\lambda_{Raman}) N(E_I) \sigma_R I_{exc}(\lambda_{exc}) \\ & + \eta_{OM}(\lambda_{exc},\lambda_{Raman}) I_{exc}(\lambda_{exc})[1 - T_{OM}(\lambda_{Raman})]. \end{aligned} \tag{9}$$

Here, I_S is the Raman scattered light intensity, $N(E_I)$ is the concentration of MP molecules, σ_R is the Raman scattering cross section, and I_{exc} is the laser excitation intensity. No assumptions regarding photoreceptor bleaching have to be made, and since the fluorescence of the lens is easily distinguishable from the spectrally sharp Raman

response of MP, it can be easily subtracted. On the other hand, since very little MP exists outside the macula area, foveal Raman measurements cannot be referenced to perifoveal levels, and lens absorptions as well as all anterior media scattering will reduce the observed Raman intensities.[11,14,15]

3. SINGLE-EXPOSURE MACULAR PIGMENT IMAGING—EXPERIMENTAL PROCEDURES AND VALIDATION TESTS

We based our MP measurements on an experimental configuration involving direct, large diameter, laser excitation of a foveal and peripheral macular spot, using an imaging CCD camera for fluorescence detection.[39] The setup is shown schematically in Fig. 4. It is designed to maximize the throughput for fluorescence originating from the retina. Two fiber-coupled solid state lasers are sequentially used as excitation sources. They operate at 488 and 532 nm, respectively, and are controlled by a computer-interfaced mechanical shutter. At the fiber output, the laser beams are expanded, collimated with an achromatic lens L1, filtered by a narrowband interference filter F1 (FWHM ~1 nm), and projected onto the retina using a lens L2, a dichroic holographic beam splitter BS1, and the human eye lens. The resulting excitation disk on the retina is ~3.5 mm in diameter. The excitation disk has an intermediate focus at the position of an aperture AP that is positioned in front of the eye (~1 cm distance) and that effectively blocks spurious reflections originating from beam splitter BS1. To ensure steady fixation of the eye during measurements, a red aiming laser is used as the fixation target. It is routed into the setup with an uncoated quartz beam splitter BS2. The fixation light is directed either to the fovea, for measurements centered on the fovea of the macular region, or to the peripheral macula (~7° eccentricity). The fixation laser beam diameter on the retina is ~200 μm. The optical shutter is designed such that it transmits a small portion of the excitation light even when it is closed. This allows the subject to view both the red fixation target and the superimposed laser excitation disk for optimum head alignment, which is further facilitated by an adjustable chin rest. At prolonged viewing, the leaked excitation light (6.9 log trolands) effectively bleaches more than 90% of the photoreceptor pigments of the macula. This establishes uniform background absorption throughout the exposed retina. The lipofuscin fluorescence is routed through beam splitter BS1, which is transparent for wavelengths above ~580 nm, through holographic notch filter F2, which blocks excitation light wavelengths, and through a long-pass filter F3, which becomes transmissive above 700 nm. Limitation of the fluorescence to wavelengths above 700 nm ensures rejection of light from unwanted fluorophores such as the lens and provides optimum contrast between peripheral and macular fluorescence intensities, as shown below. Finally, the signal is collected by a 50 mm focal length achromat L3 and imaged onto the 512×512 pixel array of a CCD camera (Model ST-9 XE, Santa Barbara Instrument Group, Inc.). Individual pixel dimensions are 20 μm height by 20 μm width; quantum efficiency in the red/near IR drops slowly from 60% at 650 nm to 40% at 800 nm. The instrument is interfaced to a computer that controls the shutter and acquires data via software supplied by the camera manufacturer. For data analysis, the pixel intensity maps are converted to proportional files, and they are further processed with suitable image processing software (The MathWorks, Inc.). Measurements were performed with undilated eyes in a darkened room. Background noise levels were typically in the range of 100 counts per pixel; signal counts typically amounted to ~30,000 counts per pixel. The CCD camera temperature was kept at ~−10 °C during measurements. Laser speckle in the images was effectively removed by mechanically shaking the light delivery fiber during measurements, which generates a spatially homogeneous laser excitation spot via fiber mode mixing. The resulting speckle removal effect is illustrated in Fig. 5 for images of millimeter graph paper and the macular area of a human retina, respectively, demonstrating that fine details such as small retinal blood vessels in the peripheral macula can be resolved. Since a 1 mm distance is imaged onto a pixel array distance of 120 pixels, we estimate an ~10 μm spatial resolution under the used imaging conditions after speckle removal.

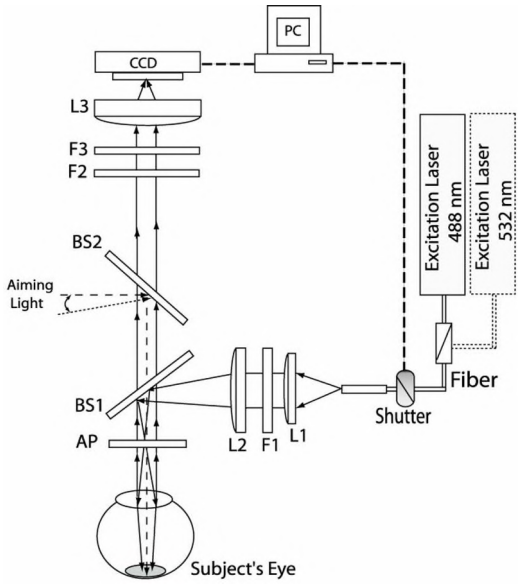

Fig. 4. Schematics of experimental setup used for imaging MP distributions in living human subjects. L1, L2, L3, lenses; F1, narrow bandwidth laser line filter; BS1, dichroic beam splitter; BS2, uncoated quartz beam splitter; AP, aperture; F2, F3, emission filters; CCD, charge-coupled detector array; PC, personal computer. A red aiming laser serves as a fixation target; depending on its direction, images can be recorded for either the macular region or the peripheral retina.

For correct imaging of large tissue regions, and for the purpose of comparing MP measurements for single-wavelength (488 nm) and dual-wavelength (488 and 532 nm) measurements, intensity corrections have to be made that account for intensity variations of the Gaussian-shaped laser beam profile and the resulting fluorescence response across the excitation spot. To illustrate this point, we imaged the lipofuscin distribution in the peripheral macula and in the foveal area by using an ~3.5-mm-diameter excitation spot. As seen from Fig. 6, the measured lipofuscin intensity distribution follows

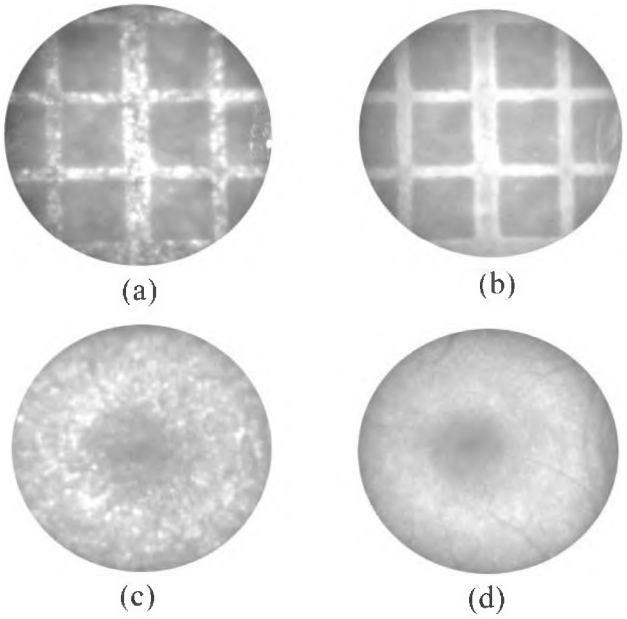

Fig. 5. Removal of laser speckle effects in fluorescence imaging, illustrated for [(a) and (b)] gray-scaled images of millimeter graph paper and [(c) and (d)] MP distributions. Granularity of images is removed in (b) and (d) when scrambling the excitation light via fiber mode mixing. This makes it possible to resolve fine details in the retinal images such as small retinal blood vessels at the periphery of the macula [(d)]. Calibrating the image dimensions with the known pixel array dimensions (1 mm equals 120 pixels), we see that retinal blood vessels as thin as ~20 μm can be clearly resolved in the used setup.

again a Gaussian beam profile, dropping for both wavelengths (488 and 532 nm) by ~20% from the central intensity level to a reduced level at the periphery of the fluorescence image. Thus fluorescence intensity levels at the edge of the image disk have to be multiplied by a corresponding correction factor (~25%) before comparing them with central image values. To eliminate the potential for any deviations from these profiles in living human eyes due to scattering and absorption effects of the anterior ocular media, we decided to image the lipofuscin distribution of the retina in two specific locations. As sketched in Fig. 6, one of the two images is centered on the fovea. It is recorded for this centrally fixated subject such that a 7° eccentric location, termed S, is recorded along with the fovea, F. Subsequently, a second image is recorded, which is now centered on the same peripheral location S, achieved by having the subject fixate on the aiming laser that has been changed in direction by 7°. Since the spot S has an unchanging lipofuscin concentration, any detected difference in fluorescence intensities originating from the spot S in the two images has to be due to the laser excitation intensity beam profile plus the combination of scattering and absorption effects of anterior ocular media. Comparing the corresponding intensities of the two images, we can easily derive a spatial correction factor map for each subject.

Laser power levels at the cornea were 2 mW during measurements; exposure times were 200 ms. At a retinal spot size of 3.5 mm diameter, the light exposure was thus about 3 mJ/cm^2, which is approximately a factor of 3 below the photothermal safety limit of 10 mJ/cm^2 set forth by the ANSI standard.[40] The photochemical limit for retinal injury is listed in the same standard as 15.5 J/cm^2 for the used wavelengths. At the used energy density of 3 mJ/cm^2, the exposure is therefore a factor of ~5000 below the photochemical limit. Sequential measurements of a subject at 488 and 532 nm could be carried out within a short measurement time of about half a minute following eye/head alignment with the help of a chin rest. The time interval between 488 and 532 nm image acquisition was about 2 min, allowing for fading of afterimages.

Typical retinal lipofuscin fluorescence images, "pixel intensity maps I_{488} and I_{532}," obtained at near IR wavelengths ($\lambda > 700$ nm) from the macular region of the retina under 488 and 532 nm light, respectively, with the exposure conditions described above, are shown in Fig. 7. The two images differ substantially in the macular region, showing pronounced absorption due to MP under 488 nm light and virtually no absorption under 532 nm light excitation, as expected from the MP absorption behavior (see Fig. 1). We used small blood vessel patterns in these images (see Fig. 7 and also Fig. 15 below) as landmarks to align these two distributions for digital image processing. We use the lipofuscin fluorescence intensity map obtained under 532 nm excitation, I_{532}, to assess the distribution of the lipofuscin and melanin concentration throughout the retinal area of interest, i.e., the area centered on the fovea and subtending to ~7° eccentricity. This is the case since the I_{532} intensities decrease from the macular image location with $I_{max,532}$ to the peripheral location with $I_{min,532}$ by only the known correction factor

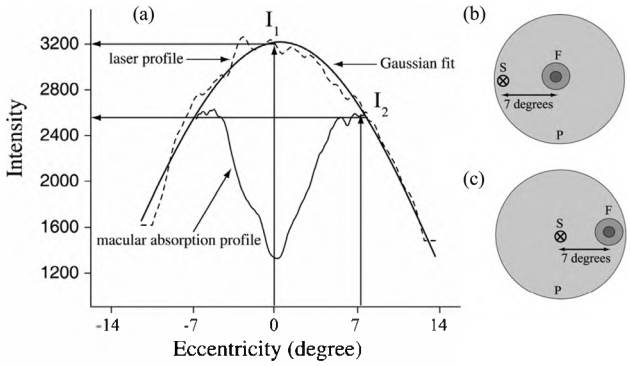

Fig. 6. Determination of spatial correction factor for image processing due to spatially varying intensities in laser excitation and lipofuscin fluorescence disks. (a) Lipofuscin fluorescence intensity in the peripheral retina, plotted versus distance along horizontal meridional line running through the center of a ~3.5 -mm-diameter image disk (solid curve). The intensity profile has a good match to a Gaussian fit (dashed curve), as expected for the Gaussian intensity profile of the exciting laser disk. At the edge of the spot the intensity has dropped by ~20% with respect to the center of the profile. This value is used as a correction factor. (b) and (c) Schematics of central and peripheral retinal images recorded sequentially for measured eyes. In image (b), the excitation disk is centered on the fovea F, and in image (c), it is centered on a spot S in the peripheral retina that is 7° eccentric. Spot S is visible in both images. Since the spot has a constant lipofuscin concentration, the fluorescence intensities originating from it in images (b) and (c) have to be due to the excitation intensity profile, and the intensity difference can be used as a spatial correction factor in the determination of MP levels from image (b) or (c).

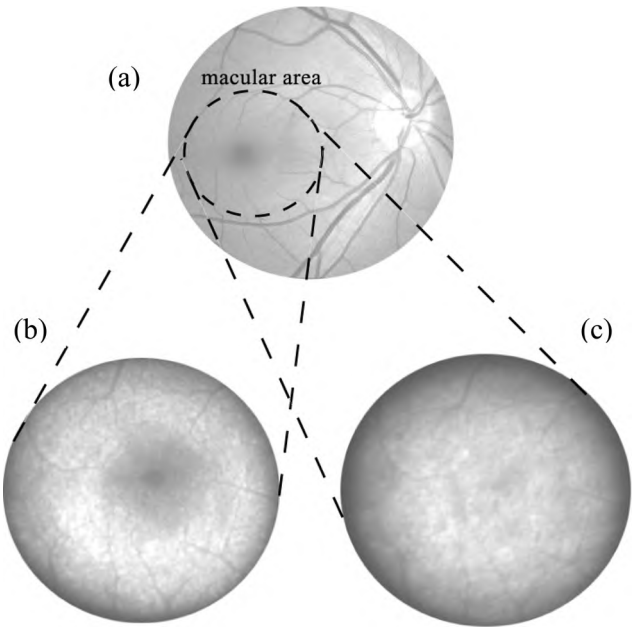

Fig. 7. (a) White-light fundus camera image of a healthy subject (a), and lipofuscin fluorescence images of the fundus obtained at near IR wavelengths with (b) 488 nm and (c) 532 nm laser excitation. Note the pronounced attenuation of fluorescence in the center of image (b) due to MP absorption and the nonattenuated fluorescence in image (c). Pixel intensity maps of images (b) and (c) are used for an indirect derivation of MP concentration levels existing in the macular region (see the text).

c_{Gauss} (this factor is described above and is due to the combined Gaussian laser excitation and fluorescence response profile).

Next, to derive the MP optical density in the fovea or surrounding regions, we use the measured lipofuscin fluorescence intensity maps obtained under 488 and 532 nm excitation, respectively, to determine the MP optical density difference from Eq. (8), which becomes

$$\mathrm{O.D.} = 1.2 \times \left[\log\left(\frac{\bar{I}_{\max}}{\bar{I}_{\min}}\right)_{\lambda=488} - \log\left(\frac{\bar{I}_{\max}}{\bar{I}_{\min}}\right)_{\lambda=532} \right], \tag{10}$$

where $\bar{I}_{\max}$ and $\bar{I}_{\min}$ are intensities averaged over certain pixel areas (see below). The factor 1.2 takes into account the ratio between the absorption of MP at its maximum (460 nm) and the used excitation wavelengths of 488 and 532 nm. We determined this factor from the absorption spectrum of MP measured from an excised eye cup.[11]

For the calculation of average MP levels in specific locations or along nasal–temporal and inferior–superior meridians, we group individual pixels into disks with a diameter of 20 pixels each, as illustrated in Fig. 8. Averaged peripheral pixel intensities are determined from 12 peripheral pixel disks located on a circle with 7° eccentricity to the fovea, and the average pixel intensity in an area of interest is determined from an additional, single disk positioned in that area, for example in the fovea, as shown in Fig. 8.

To test our experimental setup and the image processing routines, we imaged a tissue phantom in exactly the same geometry and under the same conditions as those used for living eye measurements (180° detection geometry with CCD camera detection), including identical light filtering and pixel processing. The tissue phantom consisted of a dried drop of lutein solution spotted onto one of the side windows of a thin-walled cuvette filled with a methanolic A2E solution,[41] as illustrated in Fig. 9. The optical density of the solution had a value of 0.35 and 488 nm. The dried lutein spot was roughly circular in diameter (~2.5 mm) and had a nonuniform thickness and concentration that increased from the center outward. Using a small diameter (200 μm) 488 nm laser excitation spot, we imaged the lipofuscin fluorescence intensity of the lutein spot/A2E solution combination, or the A2E solution alone, progressing from the center of the lutein spot toward the periphery and beyond. Simultaneously, we also measured the *in situ* sample transmissions at the laser wavelength, using a light chopper in the excitation laser beam, and phase-sensitive detection of the transmitted laser beam with a silicon photodetector placed behind the tissue phantom. From these measurements we were able to directly correlate lipofuscin-emission-based optical densities of local lutein concentrations inside the phantom spot with optical density values obtained from transmission data. The results are displayed in Fig. 9 for a few dozen locations within the lutein spot. They demonstrate excellent agreement between the two methods (correlation coefficient $R=0.96$), proving that the imaging procedures and data processing routines lead indeed to the desired lutein optical density determination for this tissue phantom.

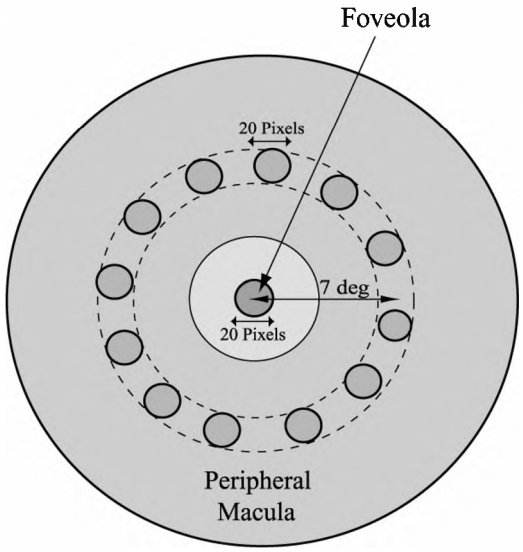

Fig. 8. Schematics showing processing of CCD pixel intensity regions to derive optical density values of MP absorption at any desired location in the retina. Individual pixels are grouped into disks with a diameter of 20 pixels each, and the intensities in these disks are averaged. One central disk is located at the center of the macula, the faveola, with a resulting intensity $I_{min}(ave)$. Twelve additional disks are chosen on a circle with 7° eccentricity to the foveola, with equidistant spacing, to calculate an average fluorescence intensity $I_{max}(ave)$ in the periphery. The maximum MP image contrast, derived from these two averaged intensities, is proportional to the optical density of MP in the center of the macula, according to Eq. (10). Disks between the center and the peripheral circle (not shown) can be chosen to calculate the image contrast and MP at any eccentricity toward the peripheral retina.

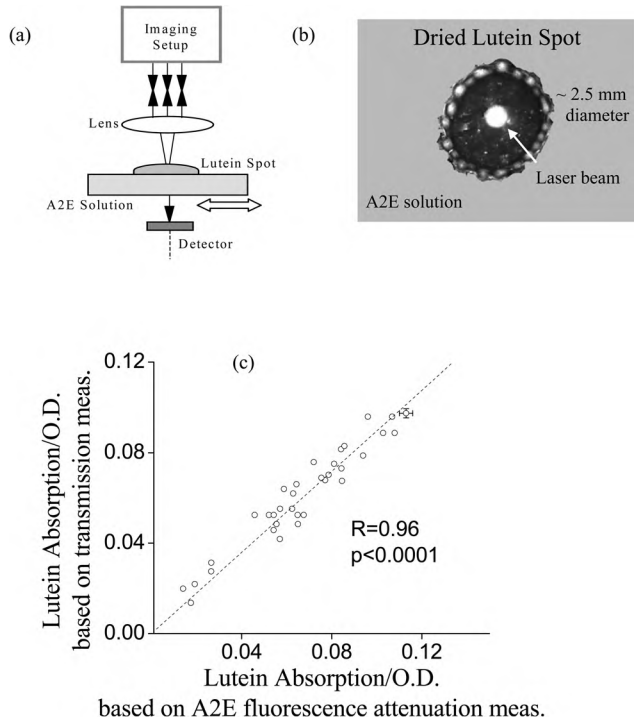

Fig. 9. Measurement of lutein concentrations in a tissue phantom consisting of a dried lutein spot located on the side wall of a thin cuvette filled with an optically thin A2E solution (O.D. ~0.35). Optical densities of lutein concentrations were measured for several dozen positions within the lutein spot, using simultaneous lipofuscin fluorescence attenuation and transmission measurements of the individual spots. The dried lutein spot increased in thickness toward its periphery, thus providing a test sample with increasing strongly varying absorptions. Setup shown (a) schematically in side view and (b) from top. (c) Lutein optical densities measured with both techniques, showing excellent correlation (correlation coefficient $R=0.96$). Transmission-based absorption levels had an accuracy of 2%; indirect, lipofuscin-based absorption levels had an accuracy of 4%.

For the determination of the MP optical density, the obtained image contrast is obviously the key parameter, being directly proportional to the MP optical density. In living eyes, care must be taken that the lipofuscin fluorescence image contrast is not artifactually reduced or enhanced by absorbing or fluorescing compounds other than MP. For example, if an artifactual fluorescence signal existed in the macula, it would add to the fluorescence level of lipofuscin and thus reduce the image contrast. Likewise, an extra fluorescence signal in the periphery, or an absorption in the center from unbleached photoreceptors, would enhance the image contrast. A presence of artifacts would be obvious if there were to be a wavelength dependence of the obtained image contrast, i.e., if the image contrast were to change depending on which spectral portions of the lipofuscin fluorescence were included in the measurement and subsequent derivation of the MP levels.

To check for the existence of artifacts, we carried out a series of measurements in which we limited the detected lipofuscin fluorescence signals to progressively longer wavelength regions. Using long-wavelength step function transmission filters with successively longer cut-on wavelengths with the two-wavelength measuring scheme (488 and 532 nm), and testing the effect on three subjects, we obtained the MP results shown in Fig. 10. The optical density values were computed with Eq. (10) and included correction of the respective digital images for laser intensity variations within the excitation disk (c_{Gauss}). We observe enhancement factors of 1.71, 1.72, and 1.85, respectively, of the image contrast at wavelengths limited to 700 nm and beyond, as compared with MP levels obtained when including fluorescence components in the blue–green spectral region. The variability of the results in Fig. 10 did not correlate with the age of the subjects. To test whether the interfering green fluorescence component originates from intrinsic MP fluorescence (see Fig. 1 for the emission spectrum), we imaged an excised eye cup from a donor eye, using essentially the same imaging setup as that for living eyes. We obtained an MP O.D. value of ~0.4±10% for this sample throughout the wavelength range 530–700 nm, thus revealing an absence of a wavelength effect on the optical density. This proves that intrinsic MP fluorescence is too weak to interfere with the obtainable image contrast of the lipofuscin-fluorescence-based imaging technique. Next, we measured the wavelength dependence for the foveal MP levels of a subject having an implanted, nonfluorescing prosthetic eye lens. Again, we observed an absence of a wavelength effect over the range 530–700 nm. From these results we conclude that the artifactual green fluorescence present in living eyes originates from fluorophores present in the living eye lens. For the purpose of obtaining optimum image contrast and corresponding MP level determination, we find it important, therefore, to detect fluorescence levels only on the long-wavelength shoulder of the lipofuscin fluorescence, i.e., above ~700 nm. These experiments and results confirm similar conclusions by Delori *et al.*[25] that detection at long wavelengths (detection window centered at 710 nm in his case) minimizes the effects of secondary fluorophores.

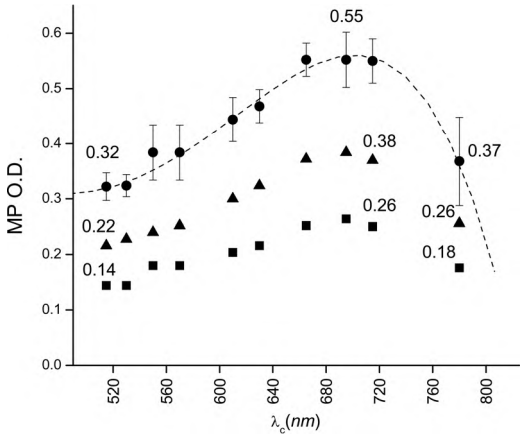

Fig. 10. Wavelength dependence of MP optical density obtained when successively limiting the detected fluorescence range to longer wavelengths, using long-wavelength pass filters with suitable cut-on wavelengths λ_c. The effect was measured for three subjects. Optimum image contrast and resulting maximum MP optical density are obtained when limiting the detection of lipofuscin fluorescence to wavelengths $\lambda \geq 700$ nm. Note the strong reduction of MP optical density, caused by decreased image contrast when including green–yellow wavelengths. The effect is caused by artifactual emission signals in that wavelength region originating from the human lens.

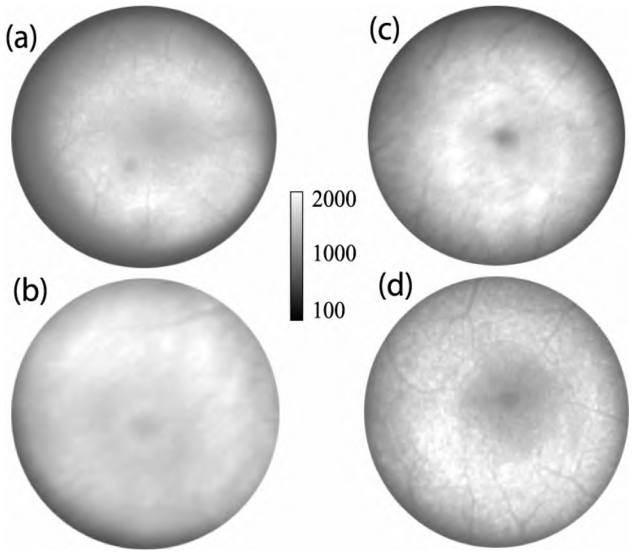

Fig. 11. Lipofuscin fluorescence images of four volunteer subjects [(a)–(d)], obtained under 488 nm excitation, shown in gray scale. Fluorescence intensities are lowest in central dark image regions due to absorption of excitation light by MP. Note the pronounced variation of MP distributions regarding strength, symmetry, and spatial extent among individuals.

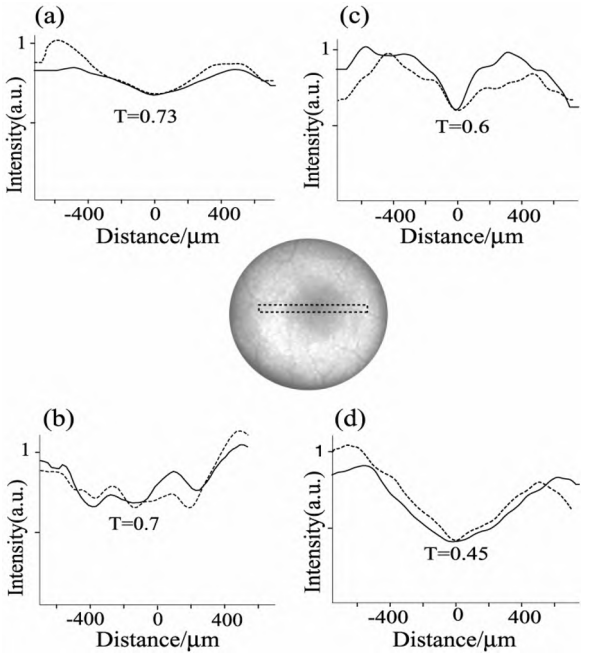

Fig. 12. Lipofuscin fluorescence intensity profiles along nasal–temporal meridians (solid curves) and inferior–superior meridians (dashed curves), all running through the center of the macula (see the inset). Plots are derived from pixel intensity maps of Fig. 8 for each of four subjects [(a)–(d)]. A transmission value in the foveola can be calculated from the averaged pixel intensities in the peripheral macula and the foveola.

In Fig. 11 we show representative MP imaging results for four healthy volunteer subjects, labeled (a)–(d), with the obtained spatial MP distributions displayed as gray-scaled intensity levels with 16 bit accuracy. All experiments were carried out with 488 and 532 nm imaging and corrected for spatial laser intensity variation over the excitation disk (c_{Gauss}). In Fig. 12 intensity line plots are displayed that are derived from the gray-scale images for each subject along nasal–temporal and inferior–superior meridians, both running through the center of the macula. In Fig. 13, the MP optical density data are plotted for each subject along the nasal–temporal meridian, and in Fig. 14, we display pseudocolor-scaled three-dimensional MP distributions derived from the two-dimensional gray-scaled intensity maps. In the line plots of Figs. 12 and 13, pixel intensities were averaged over 14 pixels (280 μm) oriented perpendicularly to the respective meridians, and transmission values were calculated versus distance from the fovea. For one of the subjects, the MP distribution was imaged eight times over a period of four weeks, showing that the MP optical densities could be determined with a test–retest accuracy (standard deviation) of 2.4%.

As can be clearly seen from Figs. 11–14, the spatial widths, symmetries, and concentrations of MP vary significantly among the four subjects. In subject (a), the MP distribution shows only a weakly enhanced central level compared with the parafovea. In subject (b), the MP distribution has a very low central level and is surrounded by a ring of MP. Subject (c) has a strongly peaked MP distribution in the center and almost no parafoveal levels, and subject (d) has both high central and parafoveal MP levels.

To investigate the influence of blood vessels on the spatial MP asymmetries, we processed the measured pixel intensity maps with reduced vertical pixel averaging, and with filter masks to enhance finer spatial details. Two gray-scale images and corresponding nasal–temporal meridional line plots illustrate the results. They are shown in Fig. 15. In the image shown at the top of the figure, the pixel intensity map is unfiltered. In the image shown at the bottom, the map is filtered and weighted with a Gaussian mask. For both images, resulting transmission line plots are shown, resulting from averaging over 15 pixels (solid curves) and 5 pixels (dashed curves), respectively. Averaging of 15 vertical pixels produces smooth curves but reveals pronounced asymmetries in the shoulders of the distribution at ~400 μm eccentricity. Averaging of only 5 pixels results in a clearly visible spa-

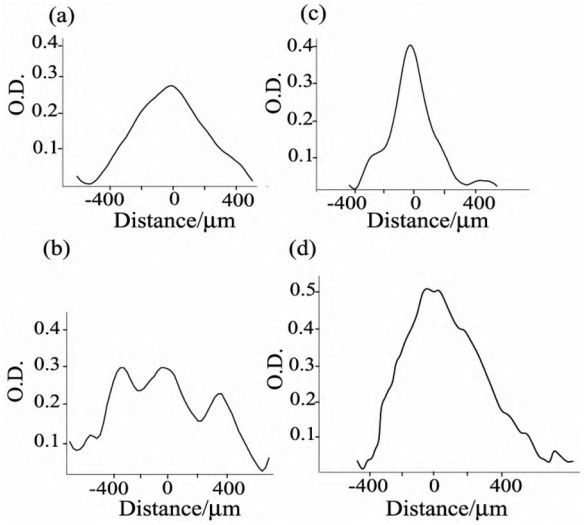

Fig. 13. MP optical density plot profiles along horizontal axis, derived from Fig. 11 for each subject.

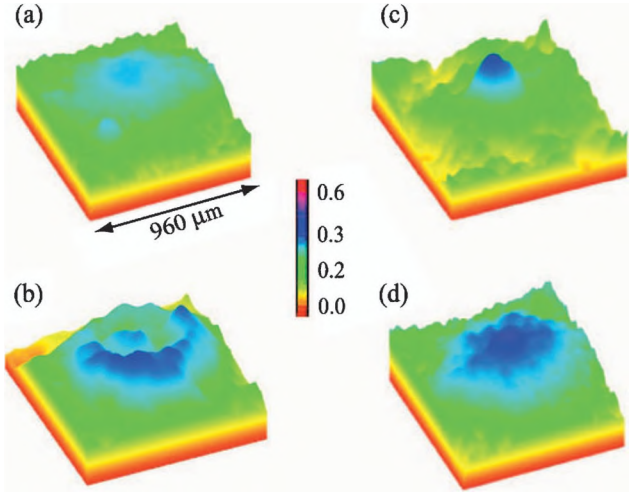

Fig. 14. Pseudocolor-scaled, three-dimensional MP distribution derived from two-dimensional lipofuscin fluorescence pixel intensity maps of Fig. 8. Note the significant intersubject variations in MP levels, symmetries, and spatial extent.

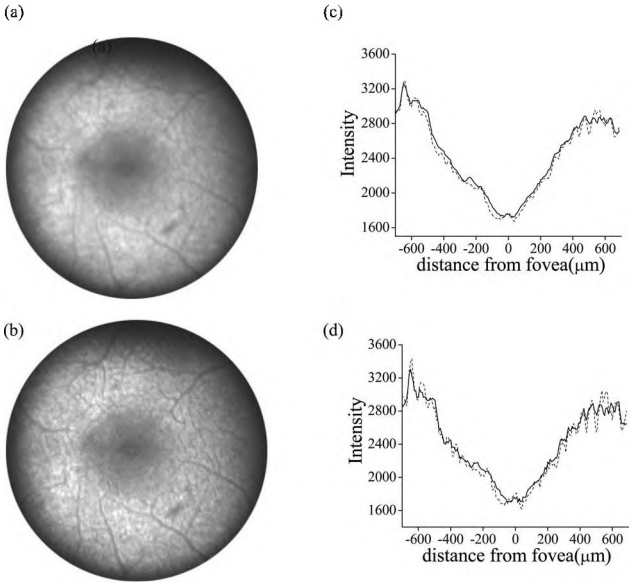

Fig. 15. Effect of blood vessels on transmission line plots derived from gray-scale lipofuscin fluorescence intensity maps. Two lipofuscin fluorescence images are compared: (a) a standard gray-scale image and (b) the same image convoluted with a mask filter, revealing finer details. For both images, nasal–temporal transmission plots are calculated and shown in (c) and (d), respectively, for rectangular pixel areas of 5 pixels height and 150 pixels width (dashed curves) and 15 pixels height and 150 pixels width (solid curves). The appearance of small blood vessels on the order of ~50 μm diameter (~2 pixels) is clearly seen in the wings of the MP profile. The spatial asymmetry of the profile, however, is not influenced by the blood vessels. Note the small dip in absorption of MP in the faveola for this subject.

tial fine structure (~50 μm width) in the shoulders of the MP distribution, as evidenced by large amplitude oscillations in the profile in the ~300–600 μm eccentricity range. The overall spatial asymmetry of the profile, however, is not influenced by the blood vessels. In the higher resolution plots, other spatial details not related to blood vessels are discernible, too, such as the small but clearly resolved dip of the MP absorption profile in the foveola of this subject.

4. CLINICAL RESULTS

To further evaluate the lipofuscin-fluorescence-based MP imaging technique, we carried out a clinical population study involving 70 healthy volunteer subjects, recruited from ophthalmology clinics at the University of Utah Moran Eye Center. All patients signed Institutional Review Board approved consent forms. The demographic characteristics of the patient population are shown in Table 1.

In Fig. 16 we display distinctive MP distribution patterns observed in these subjects. We distinguish five categories, A–E, based on striking spatial features in the MP distributions. In category A, MP optical densities were very low (smaller than ~0.05). This is observed for 11% of the population sample. In category B, the MP distribution is laterally extended and has enhanced central MP levels; it is seen in 22% of the subjects. Category C features only a sharp central MP distribution, which is seen in 28% of the subjects. Category D has a sharp central MP distribution and an additional MP ring located in the parafovea; this pattern is seen in 17% of the subjects and has been previously noted by other investigators using autofluorescence and reflectometry.[42] Finally, category E has a relatively uniform, laterally extended MP distribution with no elevated central MP levels, a pattern seen in 12% of the subjects. We did not investigate a potential relationship between the distribution types and age and gender, since this type of analysis would ideally have a larger subject population to reach statistical significance.

For 20 of the subjects, we recorded images for both 488 and 532 nm excitation and evaluated the MP levels according to Eq. (10). However, in all subjects an image contrast due to MP concentrations was practically absent under 532 nm excitation. The images all looked very similar to that shown in Fig. 7 and contributed at most 5% of the contrast relative to that observed with 488 nm excitation. From this, we concluded that 532 nm images are not essential for MP determinations in healthy subjects, and to facilitate rapid scanning of this clinical population sample, we used only single-wavelength, 488 nm measurements for the remaining subjects. It is clear, though, that two-wavelength imaging is required to achieve highest accuracies, and it is very likely to be required also for subjects with pathologies.

In Fig. 17, we display MP levels obtained for each subject as a function of age. For each subject the data point corresponds to a central MP level obtained by integrating the respective image over its foveolar region (150 μm diameter). At any age, there can be a large variation of MP levels. In several subjects with age near 40 yr, for example, the MP levels are seen to range from an O.D. near

Table 1. Demographics of the Population

Number of normal subjects	70
Age (yr: mean±SD)	53±16
Age range (yr)	23–89
Female (%)	50
Male (%)	50
Caucasian Subjects (%)	90
Nonsmokers (%)	86
Active smokers (%)	14

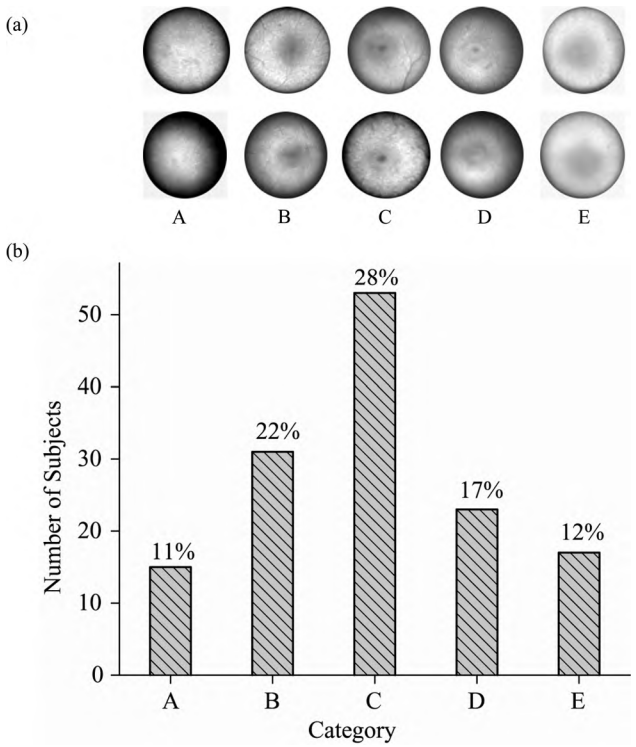

Fig. 16. (a) Categories of MP distributions observed in clinical measurements of 70 subjects. Two examples are shown for each category. Category A has very low MP levels (O.D. smaller than 0.05), B features enhanced central MP levels and lower eccentric levels, C has only a sharp, central MP distribution, D has a central MP concentration surrounded by lower amounts arranged as a ring or shoulder, and E has both central and parafoveal MP levels. (b) Distribution of 122 measured eyes among categories A–E. A large fraction of subjects, 28%, has a sharp, central MP distribution.

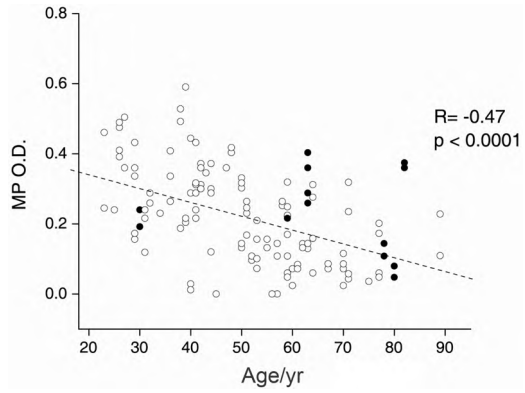

Fig. 17. MP levels measured in 90 eyes of a clinical population of 70 volunteer subjects, displayed as a function of age. Each data point corresponds to the maximum MP level determined from lipofuscin fluorescence images. Note the significant variation of MP levels among individuals at any age and the average decline of levels with age. Solid circles represent subjects measured after cataract surgery (lens implant).

zero to an O.D. of ~0.6. Also, there is a statistically significant decline of average MP levels with increasing age, with a correlation coefficient $r=-0.47$. Calculating the correlation coefficient with one data point per subject (one eye per subject), we obtain $r=-0.54$. The decline with age is similar to MP results obtained with resonance Raman detection in previous Utah population studies studies[11,43] and in an Irish study[44] but differs from other previous reports, which also used autofluorescence imaging.[25,32]

Finally, we investigated the correlation of the indirect, lipofuscin-fluorescence-based MP detection technique with the direct technique of integral resonance Raman detection, the latter measuring MP responses over a ~1.2-mm-diameter excitation spot in an integral fashion.[11] For this purpose we recruited a clinical population subgroup of 48 subjects and measured 72 eyes. The results are shown in Fig. 18, revealing a statistically significant and strong correlation between both methods (correlation coefficient $r=0.73$, $p<0.0001$, including all eyes measured; and $r=0.75$, $p<0.0001$, including only one eye per subject). Solid circles in Fig. 18 correspond to data points for subjects with lens implants. Limiting the correlation to MP optical densities below ~0.35, the correlation is even stronger. At optical densities above ~0.35, the variance of the levels increases, likely caused by breakdown of the assumptions underlying the lipofuscin-based MP detection method and the resonance Raman methods.

5. CONCLUSION

Detection of lipofuscin fluorescence, in combination with suitable signal processing, appears to be a viable noninvasive objective optical method that is well suited to indirectly derive the concentrations and spatial distributions of MP in living human subjects, at least in subjects that are free from macular pathologies. Since the method is not highly molecule specific, care must be taken to eliminate confounding effects of fluorophores in the detected

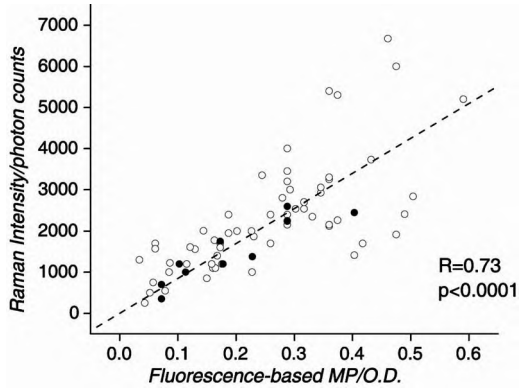

Fig. 18. Correlation between MP levels determined by lipofuscin-fluorescence-based imaging and resonance Raman spectroscopy. 72 eyes of 48 subjects were measured for these experiments. Fluorescence-based MP optical density levels are maximum levels at the foveola, calculated from lipofuscin fluorescence pixel intensity maps integrated and averaged for a circular area, centered at the fovea, having 20 pixel diameter (150 μm). Raman-based MP levels are derived from Raman scattered light intensities at the carbon double stretch frequency of 1525 cm^{-1}. Since the latter are obtained with a 1-mm-diameter, 488 nm laser, excitation spot centered on the macula, Raman-based MP levels are averaged over a 1-mm-diameter area. A remarkably high correlation (correlation coefficient $r=0.73$) is obtained between both methodologies. Raman-based levels are not corrected for media opacities, while fluorescence-based levels are not influenced by media opacities. The high correlation therefore demonstrates indirectly that media opacities are not very significant in Raman measurements.

intensity maps. We show that confounding effects can originate from fluorophores in the living human lens, which under simultaneous excitation with the lipofuscin molecules generate a strong fluorescence in the green–yellow wavelength range. The confounding effect on the optically detected MP levels can be avoided by using a transmission filter in the fluorescence detection channel that limits the detection to wavelengths on the long-wavelength shoulder of the lipofuscin fluorescence spectrum. Using a direct, CCD-based fluorescence imaging setup with laser excitation and filtered signal detection, we demonstrate that it is possible to measure MP distributions within a fraction of a second through undilated eyes with high reproducibility. MP measurements of a population sample involving 70 healthy subjects reveal distinct patterns of MP distributions, such as a pattern with high central MP levels surrounded by eccentric shoulders or rings of lower MP levels. Most importantly, it is seen that MP levels can differ very strongly among individuals, i.e., by more than 1 order of magnitude, and that the average MP levels decline slowly with age in the sampled population (on average by a factor of 3 between ages 25 and 80).

Our results also show that a single-wavelength, 488 nm laser exposure is adequate to determine the MP levels with ~95% accuracy. For most practical purposes it is therefore not necessary to use an additional excitation wavelength outside the MP absorption range for MP level determinations. However, in the presence of macular pathology, it is very likely that dual-wavelength measurements will be necessary to account for spatially nonuniform lipofuscin and melanin distributions. The fluorescence-based MP detection method shows a statistically significant correlation with MP measurements using highly MP-specific resonance Raman spectroscopy in healthy subjects, as seen from a direct comparison of both techniques in a subgroup of 48 subjects. MP levels showed a tight correlation up to integrated MP optical density levels of ~0.35. At higher MP levels, deviations occur that are likely correlated with nonlinear effects of both optical methods at higher MP levels. Possible factors include (a) screening effects in the MP Raman and lipofuscin fluorescence responses at high molecule concentrations, (b) an undersampling of the MP distributions caused by lens opacity effects in elderly subjects in the Raman method, (c) nonvanishing MP levels at the peripheral retinal reference point in the fluorescence-based method, and (d) residual absorption of photoreceptors in the fluorescence detection. We expect further insight into the differences between both methods by a direct comparison of fluorescence-based imaging results with Raman images of MP distributions in the same subjects.

Since the fluorescence-based MP detection method is not influenced, in first order, by anterior media opacities, it could have an advantage over the Raman method in elderly subjects, who in general have higher lens opacities and, according to our clinical results, also reduced MP levels. The age-related decline of MP levels confirms our earlier results obtained with the Raman detection method, although the magnitude of the decline is slightly higher in the Raman results (decline by a factor of about 5 between ages 25 and 80). In principle, this difference is not surprising, since the Raman response measures absolute MP levels and therefore is reduced by media opacities. On the other hand, the difference is very small, and therefore these comparative results show that lens opacities generate only small optical densities in the blue–green wavelength range. This is in agreement with recent literature data showing that lens optical density values are close to zero for all ages at wavelengths above ~500 nm,[45] substantially less than earlier studies had reported.[46,47] It remains unclear why the age-related decline of MP levels has not been observed by other groups using the lipofuscin-based MP detection method.[29–31] Potential explanations are that the confounding effects of lens fluorescence have not been adequately considered in those studies or that there are systematic differences in the population samples. Age-related declines in MP are consistently detected in our Utah population by three different methods—autofluorescence imaging, resonance Raman detection,[11] and heterochromatic flicker photometry[43] so our discordant findings are likely related to subject recruitment and selection factors rather than methodological differences.

In summary, spatial and quantitative information of retinal MP levels simultaneously measurable with the lipofuscin-based technique without pupil dilation can be expected to be of tremendous value in screening of large populations. It will provide a viable tool in studies investigating the influence of dietary supplements on MP levels and their distributions and in research investigating the link between MP levels and retinal pathologies.

ACKNOWLEDGMENTS

The authors acknowledge I. V. Ermakov for assistance with integral Raman measurements and D.-Y. Zhao for clinical logistical support. This work was supported in part by grants from the State of Utah (Biomedical Optics Center of Excellence grant), by Spectrotek LC, the National Eye Institute (EY 11600), and Research to Prevent Blindness (New York, New York). W. Gellermann, P. S. Bernstein, and the University of Utah hold patent rights to the Raman technology described in this article, and these authors and the university own significant equity interests in Spectrotek, LC, a company that has licensed the technology. Paul Bernstein is a Sybil Harrington Research to Prevent Blindness Scholar in Macular Degeneration Research.

Corresponding author address: W. Gellermann, Department of Physics, University of Utah, 115 S 1400 E, Room 201, Salt Lake City, Utah 84112; e-mail, werner@physics.utah.edu.

REFERENCES AND NOTES

1. M. Mozaffarieh, S. Sacu, and A. Wedrich, "The role of the carotenoids, lutein and zeaxanthin, in protecting against age-related macular degeneration: a review based on controversial evidence," Nutrition J. **2**, 20 (2003); http://www.nutritionj.com/content/2/1/20.
2. N. I. Krinsky and E. J. Johnson, "Carotenoid actions and their relation to health and disease," Mol. Aspects Med. **26**, 459–516 (2005).

3. Eye Disease Case Control Study Group, "Antioxidant status and neovascular age-related macular degeneration," Arch. Ophthalmol. (Chicago) **111**, 104–109 (1993).
4. J. M. Seddon, U. A. Ajani, R. D. Sperduto, R. Hiller, N. Blair, T. C. Burton, M. D. Farber, E. S. Gragoudas, J. Haller, D. T. Miller, L. A. Yanuzzi, and W. Willet, "Dietary carotenoids, vitamins A, C, and E, and advanced age-related macular degeneration," J. Am. Med. Assoc. **272**, 1413–1420 (1994).
5. E. Cho, J. M. Seddon, B. Rosner, W. C. Willett, and S. E. Hankinson, "Prospective study of intake of fruits, vegetables, vitamins, and carotenoids and risk for age-related maculopathy," Arch. Ophthalmol. (Chicago) **122**, 883–892 (2004).
6. C. R. Gale, N. F. Hall, D. I. Phillips, and C. N. Martyn, "Lutein and zeaxanthin status and risk of age-related macular degeneration," Invest. Ophthalmol. Visual Sci. **44**, 2461–2465 (2003).
7. R. A. Bone, J. T. Landrum, S. T. Mayne, C. M. Gomez, S. E. Tibor, and E. E. Twaroska, "Macular pigment density in donor eyes with and without AMD: a case-control study," Invest. Ophthalmol. Visual Sci. **42**, 235–240 (2001).
8. S. Beatty, I. J. Murray, D. B. Henson, D. Carden, H.-H. Koh, and M. E. Boulton, "Macular pigment and risk for age-related macular degeneration in subjects from a northern European population," Invest. Ophthalmol. Visual Sci. **42**, 439–446 (2001).
9. P. S. Bernstein, D.-Y. Zhao, S. W. Wintch, I. V. Ermakov, R. W. McClane, and W. Gellermann, "Resonance Raman measurement of macular carotenoid pigments in normal and age-related macular degeneration subjects," Ophthalmology **109**, 1780–1787 (2002).
10. T. T. J. M. Berendschot, J. J. M. Willemse-Assink, M. Bastiaanse, P. T. V. M. de Jong, and D. van Norren, "Macular pigment and melanin in age-related maculopathy in a general population," Invest. Ophthalmol. Visual Sci. **43**, 1928–1932 (2002).
11. W. Gellermann, I. V. Ermakov, M. R. Ermakova, R. W. McClane, D.-Y. Zhao, and P. S. Bernstein, "In vivo resonant Raman measurement of macular carotenoid pigments in the young and the aging human retina," J. Opt. Soc. Am. A **19**, 1172–1186 (2002).
12. T. Gillbro and R. J. Cogdell, "Carotenoid fluorescence," Chem. Phys. Lett. **158**, 312–316 (1989).
13. I. V. Ermakov, R. W. McClane, W. Gellermann, and P. S. Bernstein, "Resonant Raman detection of macular pigment levels in the living human retina," Opt. Lett. **26**, 202–204 (2001).
14. B. R. Hammond, B. R. Wooten, and B. Smollon, "Assessment of the validity of in-vivo methods of measuring macular pigment optical density," Optom. Vision Sci. **82**, 387–404 (2005).
15. W. Gellermann and P. S. Bernstein, "Assessment of the validity of in-vivo methods of measuring macular pigment optical density," Optom. Vision Sci. **83**, 254–255 (2006).
16. D. van Norren and L. F. Tiemeijer, "Spectral reflectance of the human eye," Vision Res. **26**, 313–320 (1986).
17. F. C. Delori and K. P. Pflibsen, "Spectral reflectance of the human ocular fundus," Appl. Opt. **28**, 1061–1077 (1989).
18. J. van de Kraatz, T. T. J. M. Berendschot, and D. van Norren, "The pathways of light measured in fundus reflectometry," Vision Res. **36**, 2229–2247 (1996).
19. T. T. J. M. Berendschot and D. van Norren, "Objective determination of the macular pigment optical density using fundus reflectance spectroscopy," Arch. Biochem. Biophys. **430**, 149–155 (2004).
20. N. P. Zagers, J. van de Kraatz, T. T. J. M. Berendshot, and D. van Norren, "Simultaneous measurement of foveal spectral reflectance and cone-photoreceptor directionality," Appl. Opt. **41**, 4686–4696 (2002).
21. A. E. Elsner, S. A. Burns, F. C. Delori, and R. H. Webb, "Quantitative reflectometry with the SLO," in *Laser Scanning Ophthalmology and Tomography*, J. E. Naseman and R. O. W. Burk, eds. (Quintessenz-Verlag, 1990), pp. 109–121.
22. T. T. J. M. Berendschot, R. A. Goldbohm, W. A. Klopping, J. van de Kraats, J. van Norel, and D. van Norren, "Influence of lutein supplementation on macular pigment, assessed with two objective techniques," Invest. Ophthalmol. Visual Sci. **41**, 3322–3326 (2000).
23. H. Wüstemeyer, C. Jahn, A. Nestler, T. Barth, and S. Wolf, "A new instrument for the quantification of macular pigment density: first results in patients with AMD and healthy subjects," Graefe's Arch. Clin. Exp. Ophthalmol. **240**, 660–671 (2002).
24. D. Schweitzer, G. E. Lang, B. Beuermann, H. Remsch, M. Hammer, E. Thamm, C. W. Spraul, and G. K. Lang, "Objektive Bestimmung der optischen Dichte von Xanthophyll nach Supplementation von Lutein," Ophthalmologe **99**, 270–275 (2002).
25. F. C. Delori, D. G. Goger, B. R. Hammond, D. M. Snodderly, and S. A. Burns, "Macular pigment density measured by autofluorescence spectrometry: comparison with reflectometry and heterochromatic flicker photometry," J. Opt. Soc. Am. A **18**, 1212–1230 (2001).
26. I. V. Ermakov, M. Sharifzadeh, M. Ermakova, and W. Gellermann, "Resonance Raman detection of carotenoid antioxidants in living human tissue," J. Biomed. Opt. **10**, 064028 (2005).
27. M. Sharifzadeh, P. S. Bernstein, and W. Gellermann, "Resonance Raman imaging of human macular pigment distributions" (manuscript in preparation, available from the authors: werner@physics.utah.edu).
28. F. C. Delori, "Spectrophotometer for noninvasive measurement of intrinsic fluorescence and reflectance of the ocular fundus," Appl. Opt. **33**, 7439–7452 (1994).
29. A. G. Robson, J. D. Moreland, D. Pauleikoff, T. Morrissey, G. E. Holder, F. W. Fitzke, A. D. Bird, and F. J. G. M. D. van Kuijk, "Macular pigment density and distribution: comparison of fundus autofluorescence with minimum motion photometry," Vision Res.**43**, 1765–1775 (2003).
30. M. Trieschmann, G. Spittal, A. Lommartzsch, E. van Kuijk, F. Fitzke, A. C. Bird, and D. Pauleikoff, "Macular pigment: quantitative analysis on autofluorescence images," Graefe's Arch. Clin. Exp. Ophthalmol. **241**, 1006–1012 (2003).
31. F. Delori, "Autofluorescence method to measure macular pigment optical densities: fluorometry and autofluorescence imaging," Arch. Biochem. Biophys. **430**, 156–162 (2004).
32. H. Wüstemeyer, A. Mössner, C. Jahn, and S. Wolf, "Macular pigment density in healthy subjects quantified with a modified confocal scanning laser ophthalmoscope," Graefe's Arch. Clin. Exp. Ophthalmol. **241**, 647–651 (2003).
33. M. Hammer, D. Schweitzer, and L. Leistritz, "Bestimmung der Konzentrations-verteilung des Makulapigmentes aus Reflexions- und Fluoreszenzaufnahmen," Ophthalmologe **100**, 611–617 (2003).
34. D. Schweitzer, M. Hammer, F. Schweitzer, R. Anders, T. Doebbecke, S. Schenke, and E. R. Gaillard, "In vivo measurement of time-resolved autofluorescence at the human fundus," J. Biomed. Opt. **9**, 1214–1222 (2004).
35. C. J. Kennedy, P. E. Rakoczy, and I. J. Constable, "Lipofuscin of the retinal pigment epithelium: a review," Eye **9**, 763–771 (1995).
36. N. Sakai, J. Decatur, and K. Nakanishi, "A2E: an unprecedented pyridinium bisretinoid," J. Am. Chem. Soc. **118**, 1559–1560 (1996).
37. L. E. Lamb, T. Ye, N. M. Haralampus-Grynaviski, T. R. Williams, A. Pawlak, T. Sarna, and J. D. Simon, "Primary photophysical properties of A2E in solution," J. Phys. Chem. B **105**, 11507–11512 (2001).
38. F. C. Delori, D. G. Goger, and C. K. Dorey, "Age-related accumulation and spatial distribution of lipofuscin in RPE of normal subjects," Invest. Ophthalmol. Visual Sci. **42**, 1855–1866 (2001).
39. M. Sharifzadeh, "Noninvasive optical detection of carotenoid antioxidants in the human retina," Ph.D. dissertation (University of Utah, 2005).
40. American National Standards Institute, "American national standard for safe use of lasers," ANSI Z136.1-2000 (Laser Institute of America, 2000), Sec. 8.3.

41. The sample was provided courtesy of H. Vollmer-Snarr of Brigham Young University, Provo, Utah.
42. T. T. J. M. Berendschot and D. van Norren, "Macular pigment shows ringlike structures," Invest. Ophthalmol. Visual Sci. **47**, 709–714 (2006).
43. P. S. Bernstein, D.-Y. Zhao, M. Sharifzadeh, I. V. Ermakov, and W. Gellermann, "Resonance Raman measurement of macular carotenoids in the living human eye," Arch. Biochem. Biophys. **430**, 163–169 (2004).
44. K. Neelam, N. O'Gorman, J. Nolan, O. O'Donavan, H. B. Wong, K. G. Au Eong, and S. Beatty, "Measurement of macular pigment: Raman spectroscopy versus heterochromatic flicker photometry," Invest. Ophthalmol. Visual Sci. **46**, 1023–1032 (2005).
45. N. P. A. Zagers and D. van Norren, "Absorption of the eye lens and macular pigment derived from reflectance of cone photoreceptors," J. Opt. Soc. Am. A **21**, 2257–2268 (2004).
46. J. Pokorny, V. C. Smith, and M. Lutze, "Aging of the human lens," Appl. Opt. **26**, 1437–1440 (1987).
47. G. L. Savage, Ch. A. Johnson, and D. L. Howard, "A comparison of noninvasive objective and subjective measurements of the optical density of human ocular media," Optom. Vision Sci. **78**, 386–395 (2001).